

GPSPMirror: Expanding Accurate GPS Positioning to Shadowed and Indoor Regions with Backscatter

Huixin Dong¹, Yirong Xie¹, Xianan Zhang¹, Wei Wang^{1*}, Xinyu Zhang², Jianhua He³

¹Huazhong University of Science and Technology

²University of California San Diego ³University of Essex

{huixin,xieyr997,xiananzhang,weiwangw}@hust.edu.cn, xyzhang@ucsd.edu, j.he@essex.ac.uk

ABSTRACT

Despite the prevalence of GPS services, it still suffers from intermittent positioning with poor accuracy in partially shadowed regions like urban canyons, flyover shadows, and factories' indoor areas. Existing wisdom relies on hardware modifications of GPS receivers or power-hungry infrastructures requiring continuous plug-in power supply which is hard to provide in outdoor regions and some factories. This paper fills the gap with GPSPMirror, the first GPS-strengthening system that works for unmodified smartphones with the assistance of newly-designed GPS backscatter. The key enabling techniques in GPSPMirror include: (i) a careful hardware design with μW -level power consumption that pushes the limit of backscatter sensitivity to re-radiate extremely weak GPS signals with enough coverage approaching the regulation limit; and (ii) a novel GPS positioning algorithms achieving meter-level accuracy in shadowed regions as well as expanding locatable regions under inadequate satellites where conventional algorithms fail. We build a prototype of the GPSPMirror tags and conduct comprehensive experiments to evaluate it. Our results show that a GPSPMirror tag can provide coverage up to 27.7 m. GPSPMirror achieves median positioning accuracy of 3.7 m and 4.6 m in indoor and urban canyon environments respectively.

CCS CONCEPTS

- **Information systems** → **Global positioning systems**;
- **Hardware** → *Networking hardware*.

KEYWORDS

GPS, Backscatter, Localization

Permission to make digital or hard copies of all or part of this work for personal or classroom use is granted without fee provided that copies are not made or distributed for profit or commercial advantage and that copies bear this notice and the full citation on the first page. Copyrights for components of this work owned by others than ACM must be honored. Abstracting with credit is permitted. To copy otherwise, or republish, to post on servers or to redistribute to lists, requires prior specific permission and/or a fee. Request permissions from permissions@acm.org.

ACM MobiCom '23, October 02-06, 2023, Madrid, Spain

© 2023 Association for Computing Machinery.

ACM ISBN XXXXXXXX.XXXXXXX...\$15.00

<https://doi.org/XXXXXXX.XXXXXXX>

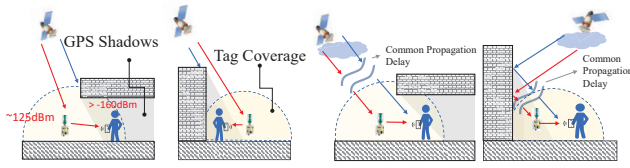
1 INTRODUCTION

Global Position System (GPS) has long been advocated as an indispensable infrastructure for many location-based services, including navigation for automobile [32, 35], pedestrian [34], ride-sharing [9], as well as asset tracking for smart factories [2]. GPS receivers generally perform well in clear line-of-sight (LoS) regions with a sufficient number of visible GPS satellites. Such an assumption does not hold in those partially shadowed regions, e.g., urban canyons, flyover shadows, and factories' indoor areas with iron sheds, where, unfortunately, navigation and tracking services are frequently needed. These services desire meter-level accuracy while positioning errors of conventional GPS in such shadowed regions often escalate to several hundred meters [9]. The U.S. Department of Transportation reports that vehicles traveling through urban areas of New York City frequently fail to obtain reliable street-level accuracy for navigation with GPS [39]. Google posits that GPS positioning in these shadowed regions remains to be "The last great unsolved GPS problem" [49].

Extensive research efforts have been devoted to tackling the challenging GPS problem. Infrastructure-based solutions, including GPS relays [13–15, 42] and DGPS stations [16, 36] are available on the market. However, such solutions typically require infrastructure support, with the dense deployment of outdoor GPS stations and/or indoor anchors, which can be expensive and labor-intensive. In particular, GPS relays and DGPS products [16] require a continuous power source and are challenging to deploy in existing urban canyons and flyover areas. Besides, laying power cables in a certain environment, such as gas factories and gas pipelines, is not allowed due to safety regulations [20].

This paper demonstrates that it is possible to leverage passive, ultra-low-power backscatter tags to enable meter-level GPS positioning for unmodified mobile devices, e.g., smartphones, in shadowed regions. As plotted in Figure 1, these backscatter tags can be deployed on walls, windows and unenclosed parts of flyovers to improve the GPS performance in shadowed regions. Our line of attack starts from the rationale that we can induce multipath in a deterministic manner

*Corresponding author.



(a) GPSMirror tag increases the number of visible satellites. (b) GPSMirror tag provides new reference propagation paths.

Figure 1: GPSMirror in shadowed regions.

using backscatter to enrich GPS propagation features that can be leveraged in positioning algorithms. Building such a system needs to fulfill requirements along following fronts:

(i) Sensitivity. GPS signals are extremely weak, i.e., below -125 dBm when reaching the Earth's surface. The backscatter tags should have a high sensitivity to effectively capture and scatter such weak incidental signals.

(ii) Coverage. To ensure sufficient coverage, the backscatter tags need to provide sufficient gain as high as regulation permits. For example, the US regulation [47] limits the coverage of a GPS repeaters' coverage within 30 m, while Europe [46] limits a GPS repeater's gain to 45 dB.

(iii) Performance and compatibility. The positioning algorithms must achieve comparable or higher accuracy compared to conventional GPS services, and should ideally require no hardware or firmware modification to existing GPS receivers (e.g., smartphones) to ensure wide acceptance.

Unfortunately, none of the existing systems meet the above requirements. On one hand, existing backscatter systems [25, 30, 45] are designed to reflect strong ambient signals, e.g., those from TV towers and WiFi access points. They cannot scatter the extremely weak GPS signals from outer space because they provide gain against the fast attenuation. While recent advances [4, 50, 51] use tunnel diodes to extend the coverage of backscatter communications, their sensitivity is still limited to around -90 dBm . On the other hand, existing GPS positioning algorithms [29, 38] are no longer applicable in our scenarios since they do not consider the extra reflection paths created by backscatter tags.

We present GPSMirror, the first backscatter-based system that introduces the following innovative techniques to meet the aforementioned requirements. Inspired by recent innovations [4, 50], we employ tunnel diode as a core component to build up the RF front-end of our low-power backscatter tag to achieve amplification with μW -level power consumption. Previous designs create carrier wave [50] or modulate their bits on incident signals [51] by employing a tunnel diode oscillator (TDO). However, our design target is completely different: we aim to carefully strengthen weak GPS signals according to regulations while preserving the original GPS waveforms with high fidelity to ensure correct decoding on smartphones. Instead, we propose a new design using tunnel diode amplifier (TDA) [37], and achieve high precision on

specific gain and bandwidth control using two resonance circuits [50]. Additionally, to achieve the extreme sensitivity, GPSMirror hinges on a series of hardware innovations, including a circularized antenna design to capture a wide range of GPS signals while reflecting them to the shadowed regions, a coupling circuit with an open loop ring (OLR) to reduce the return loss caused by the solder of circuit component in the transmission line (TL), a noise suppression design to minimize SNR degradation caused by tunnel-diode based reflective amplifier.

We design a novel positioning algorithm that takes advantage of the tag-manipulated paths to (i) achieve positioning with comparable precision to LoS GPS areas, and (ii) dramatically improve positioning precision to meter level in cases where conventional algorithms are significantly compromised (tens to hundreds of meters precision) in NLoS conditions. GPSMirror only requires the assistance of a single tag and works on smartphones as a software update without any hardware/firmware modification.

We prototype the GPSMirror tag with off-the-shelf components and benchmark its hardware performance through microscopic measurements. We further deploy GPSMirror tags in three real-world scenarios to verify their effectiveness. Experimental results show that a GPSMirror tag achieves a flat 22 dB gain in the L1 band and covers an area with a radius of about 27.7 m for smartphone reception in an urban canyon and 30 m in a corridor. The positioning algorithm achieves a median position error as low as 3.7 m in indoor scenarios and 4.6 in an urban canyon. The main contributions are summarized as follows:

(i) GPSMirror is the first backscatter system that scatters signals from orbiting satellites. The hardware design pushes the limit of backscatter in that it can re-radiate weak GPS signals as low as -125 dBm with sufficient coverage.

(ii) We propose novel GPS positioning algorithms to extend GPS positioning services in shadowed or indoor regions where conventional GPS positioning fails or is severely undermined. It works seamlessly with off-the-shelf smartphones without any hardware or firmware modification.

(iii) We implement and evaluate the GPSMirror in real-world environments using off-the-shelf smartphones from different manufacturers. Our experiments verify the feasibility and compatibility of GPSMirror.

2 OVERVIEW

The GPSMirror system comprises the hardware design of backscatter tags and the positioning algorithms on smartphones to fully use the signals re-radiated by the tags.

(i) Hardware design. We employ two key innovations to build up the GPSMirror tags: a high-sensitive RF front-end and a tunnel diode-based reflection amplifier.

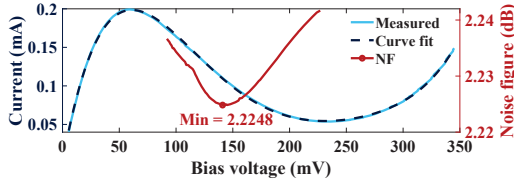


Figure 2: IV-Curve of Tunnel Diode MBD1057E28. Measured with a DC power supply (model IPS900B) and a current meter (model VC890D).

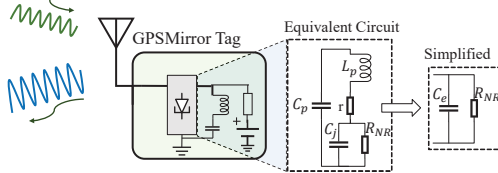


Figure 3: GPSMirror tag. GPSMirror tag enhances the injected wireless signals using a tunnel diode, which can be regarded as a combination of a negative resistance R_{NR} , parasitic capacitors and inductors.

(ii) **Positioning algorithm.** We present an algorithm to subtly use GPSMirror tags to improve the GPS positioning performance in shadowed regions. When the number of visible satellites is inadequate for conventional GPS positioning (Figure 1 (a)), we use construct virtual satellites with a single GPSMirror tag to guarantee coverage. When the number of visible satellites is adequate (Figure 1 (b)), we take advantage of the valid propagation path through GPSMirror tags to eliminate propagation errors of non-line-of-sight (NLoS) and improve accuracy.

3 HARDWARE DESIGN

This section describes the hardware design of GPSMirror tags that can scatter weak GPS signals with sufficient coverage.

3.1 Pushing Scattering Coverage to the Limit

A fundamental challenge facing GPSMirror is the dramatic attenuation when backscatter tags re-radiate GPS signals, which severely limits the coverage of the GPSMirror tags. To maximize the coverage, the tags should be able to enhance the energy of the scattered GPS signals under the regulation permit [46, 47]. Such a capability can be characterized by the standard *backscatter reflection coefficient* Γ [25, 31], i.e., the ratio of the amplitude of the reflected wave to the incident wave:

$$\Gamma = \frac{Z_L - Z_A^*}{Z_L + Z_A} = \frac{1 - Z_A^*/Z_L}{1 + Z_A/Z_L} \quad (1)$$

where Z_L and Z_A stand for the impedance of the internal circuit and the antenna, respectively. The *gain* of the backscatter tag is defined as $|\Gamma|^2$ [37]. Obviously, when Z_L is negative, the gain is greater than 1, i.e., the signals are amplified after re-radiated by backscatter tags.

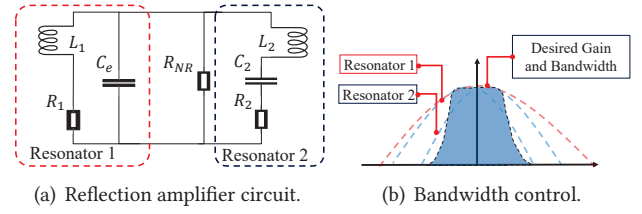


Figure 4: Reflection Amplifier. Two resonant circuits are used to match the impedance of the circuit and achieve the desired bandwidth.

To achieve this, we adopt tunnel diodes as a core component, as they can realize negative resistance with μW -level power consumption. Plotted in Figure 2 is the IV-Curve of the diode, which holds a region of negative resistance (NR) due to the quantum tunneling effect [51]. The negative resistance (R_{NR}) can be calculated from the slope of the IV-Curve. For MBD1057, which is used in GPSMirror, R_{NR} is about -650Ω in our design with a bias voltage set around $140mV$.

Classical tunnel diode was invented in the 1950s [26] and revived in recent backscatter systems [4, 50, 51] as a low power amplifier. These systems aim to use a tunnel diode oscillator to re-modulate the incident signals, e.g., in the form of low-rate ASK or FSK, which can be decoded by a specialized demodulator. In other words, the backscatter tag's modulation differs from the signal source. In contrast, GPSMirror needs to provide a high gain while preserving the incident signal's waveform. Therefore, we employ the tunnel-diode-based reflection amplifier (TDA) [12, 37] to build GPSMirror instead.

Gain and Bandwidth. The R_{NR} of the tunnel diode is about -650Ω while standard antennas' impedance Z_A is 50Ω . To realize the amplification effect according to Equation 1, we need an impedance matching network to transform the impedance of the internal circuit's Z_L to make it approach $-Z_A$.

Yet, the tunnel diode cannot simply be regarded as a negative resistance alone. Instead, it is equivalent to a combination of multiple parasitic elements, including internal junction capacitance C_j , packaging parasitic elements C_p , L_p and r , whose typical values are $0.1pF$, $0.3pF$, $1.2nH$ and 6Ω , respectively, according to the datasheet [1]. With the center frequency f_c fixed in GPS L1 band, we simplify the tunnel diode circuit by series-parallel conversion step by step and then acquire an equivalent circuit as plotted in Figure 3, where the equivalent capacitor is about $0.465pF$.

The conventional approach directly computes the overall impedance of the tunnel diode and builds a matching network. However, as the tunnel diode amplifier is susceptible to impedance changes, a straightforward search for values as in the conventional approach may introduce more parasitic parameters during manufacturing, resulting in unexpected performance.

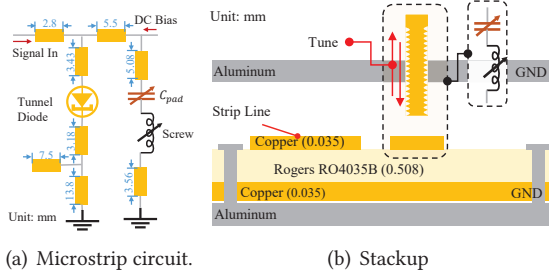


Figure 5: Structure of reflection amplifier circuit.

To address this issue, GPSMirror achieves desired bandwidth and gain by using *two resonance circuits* instead, thereby making the circuit highly repeatable and easily debugged. The first resonant circuit aims to eliminate the effects of the parasitic elements inside the tunnel diode, while the second considers the impedance changes caused by the first resonant circuit and tunes the circuit to desired bandwidth and gain. In a typical series “LC” resonator circuit, the relationship of inductance L , capacitance C and frequency f_c can be described as [56]:

$$f_c = 1/2\pi\sqrt{LC} \quad (2)$$

Given the equivalent capacitance $C_e = 0.465pF$ inside the tunnel diode, the only suitable inductance $L_1 = 2.195nH$ can be derived.

Then, the gain and bandwidth can be estimated through the quality factor Q , i.e., the ratio of resonant frequency to bandwidth, given by

$$Q = 2\pi f_c L/R \quad (3)$$

where R is the parasitic resistance inside the inductor and transmission lines. A smaller R contributes to a higher Q , and thus we use low-loss microstrip lines to route the circuit.

The second “RLC” circuit aims to achieve the desired gain and bandwidth. Given the needed bandwidth and impedance, we can determine a set of inductance and capacitance to achieve our goal according to the above equations. To ensure the gain’s flatness over the band, we slightly staggered the center frequency of the two resonant networks to ensure a consistent gain over the GPS band and sharp roll-off, which is the gain’s decreasing speed [28], beyond the band, as plotted in Figure 4 (b).

Unfortunately, integrated inductors and capacitors contain many parasitic elements along with soldering artifacts, making it difficult for circuit diagnosis. Thus, we transform the reflection amplifier circuit, as illustrated in Figure 4 (a), to practical microstrip lines on a PCB substrate to ensure the accuracy, as illustrated in Figure 5 (a). Furthermore, to deal with the PCB manufacturing imprecision that causes the resonant frequency to deviate from the design, we employ a tuning stub on board to adjust the center frequency of the first resonator and a tune pad with a tuning screw for the second one. Figure 5 (b) shows the stack-up of the

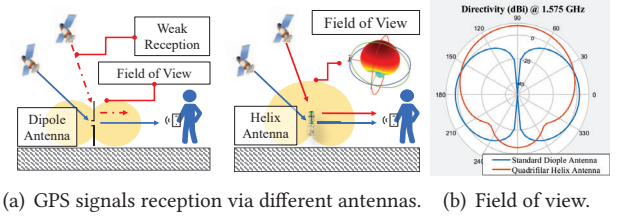


Figure 6: GPSMirror employs QHA for better fov.

GPSMirror reflection amplifier circuit. As the screw is closer to the tuning pad, the values of L_2 and C_2 increase and the resonant frequency of resonator 2 decreases, and vice versa.

3.2 High-Sensitivity RF Front-end for GPSMirror

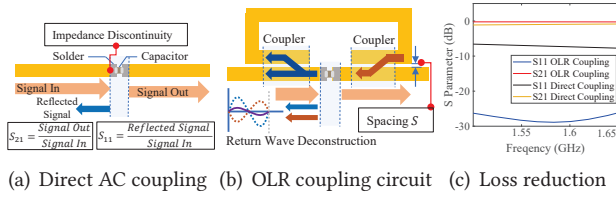
Sensitivity [33] is a measure of the magnitude of input signal needed for the amplifier to produce full output at maximum volume. To scatter GPS signals with sufficient gain, GPSMirror must be sensitive enough to acquire the weak GPS signals in the first place.

This is different from traditional passive backscatter tags which do not need to detect and amplify the incident signals and hence do not need to optimize sensitivity. It also differs from traditional radio receivers which consider the modulation/encoding gain as part of the sensitivity. In effect, the sensitivity of GPSMirror is the detector sensitivity which describes how efficiently the radiation is converted into a usable signal. We design a highly sensitive RF front-end for GPSMirror via three steps, including an antenna design that maximizes the incident signals, a low loss coupling design that reduces the return loss when the signal is coupled into the internal circuit, and a low noise amplifier design that minimizes the current noise in the circuit.

Capturing and radiating signals with a wide field-of-view (FoV). Traditional backscatters [30, 51, 57] employ dipole antennas to scatter signals within the azimuth plane. In contrast, GPSMirror reflects GPS signals over a wide 3D FoV by adapting the classical Quadrifilar Helix Antenna (QHA) structure [44].

We build the antenna with a diameter of 3.8 cm, a comparable size to GPSMirror tags. Recall that the wavelength of the GPS signal in the L1 band is valid, and the rest parameters of the antenna can be acquired from the helix antenna structure equation. we also conduct simulations in ANSYS HFSS to verify the above design choices. As plotted in Figure 8 (b), QHA significantly outperforms the standard dipole antenna in the horizontal upward direction with an average of 7.3 dB gain in all upward directions.

Reducing loss using resonant coupling. After the signals are captured by the antenna, they need to be passed to



(a) Direct AC coupling (b) OLR coupling circuit (c) Loss reduction
Figure 7: GPSMirror designs an open loop coupling circuit to reduce the return loss in the TL.

the RF front-end which may induce additional loss. A coupling circuit can be used to minimize such loss. Traditional backscatter tags use inductors and capacitors to build the matching network to couple the signals from the antennas to the internal circuit as shown in the Figure 8. However, these components need to be soldered on, which tends to damage the integrity of the transmission line (TL), resulting in the return loss, i.e., signal reflection and energy dissipation before coupling into the internal circuit.

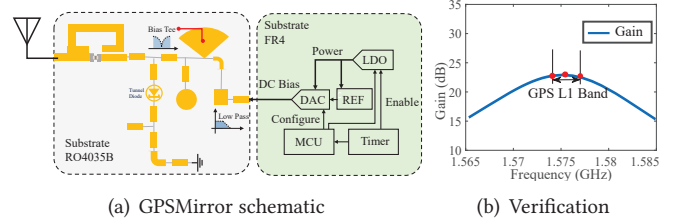
We design a new type of microstrip coupling circuit to minimize the TL loss, as illustrated in Figure 7(b). We use a microstrip couple filter, which consists of two parallel TLs, to couple the returned signal to the OLR for additional transmission delays. Intuitively, when the signal which is coupled to the OLR gets back to the pad with the opposite phase, the return signal is canceled and loss minimized. The overall length of the loop determines the phase delay, an additional $\lambda/2$ delay contributes to maximum signal deconstruction. We conduct an RF circuit simulation to verify our design. The simulation results in Figure 7 (c) show that our design significantly reduces the return loss. The S11 parameter, which is defined in Figure 7 (a), is considerably lower when compared to directly soldering a capacitor.

Operating with minimal noise. Before introducing the noise suppression design, we first describe the noise figure (NF) of the GPSMirror circuit. NF determines the degradation of SNR of the output signal compared to the incident signal, which should be minimized to maintain good signal quality. Specifically, the NF of a tunnel diode is given by [37, 54]:

$$NF = \frac{1 + K_a}{[1 - r/R_{NR}] [1 - f/f_{r0}]} \quad (4)$$

where r is the resistance of the Ge board as plotted in Figure 3, f_{r0} the cutoff frequency, f the operating frequency, $K_a \approx 1.2$ the noise factor [37], and R_{NR} the negative resistance of the tunnel diode.

As shown in Figure 2, we can fit the relationship between the bias voltage V_{Bias} and the current I with a polynomial $I = \mathcal{F}(V_{Bias})$. Thus, there is a one-to-one mapping between the voltage and R_{NR} . We thus calculate all the NF values according to Equation 4 to obtain the minimal value of NF, as plotted in the Figure 3.



(a) GPSMirror schematic (b) Verification
Figure 8: Schematic diagram and simulation result that verified the hardware performance.

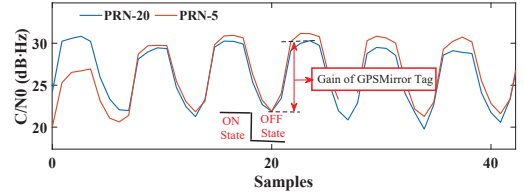


Figure 9: The amplitude feature of GPS signals that scattered by GPSMirror tag.

4 GPS-COMPATIBLE POSITIONING THROUGH BACKSCATTER SIGNALS

Conventional GPS algorithms on smartphones may perform poorly in the shadowed regions due to the following two reasons. First, inadequate visible satellites, which are caused by the obstruction of buildings, make the traditional algorithm unsolvable. Conventional GPS algorithms, however, require receiving signals from at least four visible satellites in order to estimate four unknown variables $[x, y, z, t_b]$ simultaneously [17]. Second, errors in distance measurements caused by NLoS propagation lead to inaccurate results.

Therefore, we develop a new algorithm that leverages the capabilities of GPSMirror tags to offer users the flexibility of prioritizing either extending locatable regions or improving accuracy. In this section, we first clarify the characteristics of scattered GPS signals and then proceed to describe the details of our positioning algorithm.

4.1 Features of Scattered GPS Signals

Different from traditional GPS relay systems that just amplify GPS signals to enhance the coverage, we modulate sequences on GPS signals with the “ON-OFF” switching on the GPSMirror tag. These sequences can help distinguish the scattered and non-scattered signals. Before elaborating on our algorithm design, we first introduce the accessible raw GPS measurements GPSMirror used [17]. **Signal strength measurements.** Smartphones provide the carrier-to-noise-density ratio (C/N_0) as the signal strength measurements to indicate the strength of the received GPS signal. Since the GPSMirror tags can enhance the GPS signals, the scattered GPS signals have higher C/N_0 measurements than the non-scattered signals of the same satellites. Therefore, we can

modulate significant features on C/N_0 to determine which piece of signals of which satellites have been scattered.

To discriminate the tag and extract the signal that is scattered by a GPSMirror tag, we configure the tag periodically switching between “ON” and “OFF” states to generate a certain pattern for discrimination. During the “ON” state, the DAC provides bias voltage to the tunnel diode amplifier and the GPSMirror tag starts to re-radiate GPS signals with gain; whereas the “OFF” state shuts down the bias voltage so the GPSMirror tag keeps silent. Such ON-OFF keying can significantly change the measured signal strength of GPS signals and thus changes the C/N_0 measurements on smartphones,

For a better understanding, we use a smartphone to record the C/N_0 samples with a GPSMirror tag deployed 1 m away. Plotted in Figure 9 is the measured C/N_0 from GPS satellite PRN-20 and PRN-5. The C/N_0 changes significantly with the GPSMirror tag switching from the “ON” state to the “OFF” state. We define the ratio of the C/N_0 between the “ON” state and “OFF” state is the *gain* of GPSMirror, and use this value to evaluate the coverage of GPSMirror tags in § 6.3.

Distance measurements. Smartphones provide two types of measurements related to the distance between the satellites and the smartphone: the *Pseudorange* and the *Accumulated Delta Range* measurements. The *Pseudorange* is a time-of-flight measurement calculated using the local clock of the smartphone, while the *Accumulated Delta Range* is a count of carrier cycles since the GPS sensor was started. Both measurements contain bias errors and cannot be directly used for positioning. Since we deploy GPSMirror to re-radiate GPS signals with “ON-OFF” scattering, the scattered GPS signals have additional delay t_s which is not contained in conventional GPS algorithm [21].

Pseudorange ρ of scattered GPS signals can be modeled as

$$\rho = r + ct_b + ct_s + \varepsilon_\rho \quad (5)$$

where t_b is the clock bias between a satellite and a receiver, which is the main bias error in GPS distance measurements and needs to be correctly estimated to extract accurate distance. r is the distance between the smartphone and the GPS satellite without error, c is the speed of light, and ε_ρ is the measurement error caused by other uncertain factors including ionospheric delay I , tropospheric delay T , etc. The scattered GPS signals have additional delay t_s while $t_s = 0$ for the non-scattered signals.

The distance measurements from accumulated carrier phase ϕ , denoted as $\Phi = \lambda\phi$, can typically be extracted from *Accumulated Delta Range* measurements. The relationship between Φ and r can be expressed by

$$\Phi = r + ct_b + ct_s + \lambda N + \varepsilon_\Phi \quad (6)$$

where λ is the wavelength of the GPS signals, N the phase offset relative to the initial reference phase value (commonly called ambiguity of whole cycles), and ε_Φ the measurement

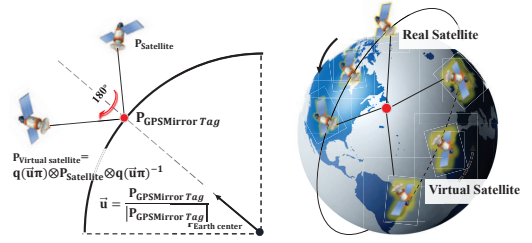


Figure 10: Position estimation of virtual satellites.

errors. Note that N is fixed since the carrier phase is kept locked by the receiver and can be estimated using a double difference of pseudorange measurements between satellites. We can estimate N by $N \approx [\Phi - \rho/\lambda]$ [27].

4.2 Extending Locatable Regions under Inadequate Satellites

Under inadequate satellite conditions (<4), the measurable propagation paths for localization are insufficient to estimate the position and clock bias. Hence, to turn these regions into locatable regions, we use GPSMirror tags to create additional measurable propagation paths through “ON-OFF” switching. To make the position estimation algorithm solvable, we then extract propagation delays through a GPSMirror tag and create “virtual satellites” that matched these measurable propagation paths. Finally, we estimate the position with combined measurements.

Estimating position of virtual satellites. To correctly solve Equation (5), the virtual satellites must comply with the following rules. (i) A virtual satellite and the real satellite that emits the scattered GPS signals need to share the same pseudorange and Doppler shift to ensure the correctness of the solution. (ii) The orbit of a virtual satellite is still a true GPS orbit. (iii) A virtual satellite needs to be far away from the real satellite to ensure a small Dilution of precision (DOP) and make the solution robust to measurement uncertainty.

To meet such requirements, we create virtual satellites by rotating the original satellites’ position vectors by 180° centered on the GPSMirror node, as shown in Figure 10. In particular, we create a virtual satellite with coordinates P_{vs} from a real satellite with coordinates P_{rs} according to the standard rotation equation [3].

Extracting the delay of scattered signals. The delay of propagation through a GPSMirror tag, t_s in Equation (5), should be extracted before positioning. Since the scattered and non-scattered GPS signals are received by the same smartphone, the clock bias remains the same. Assuming that we get nearby samples of GPS signals statically and acquire clock bias t_{b1} from non-scattered GPS signals, we presume the clock bias from scattered GPS signals t_{b2} equals to $t_s + t_{b1}$. We can estimate t_s from a pair of scattered and non-scattered GPS measurements and update the t_s with further measurements.

Positioning the receiver with a single GPSMirror tag. Combining the measured pseudorange directly from scattered and non-scattered GPS signals, we estimate the receiver's position with the weighted least squares (WLS). Below we elaborate on this process.

We first set an initial position $L_0 = [x_0, y_0, z_0] = [0, 0, 0]$ to activate the iterative algorithm, and then obtain the locations of the tracked satellites from the ephemeris, which is the GPS satellites' orbital information forecast by NASA.

Different from conventional algorithms, GPSMirror needs to calculate the distance from both the real and virtual satellites to the given initial position. Suppose m satellite signals, including real and virtual satellites, are to be acquired. For the k -th satellite ($k \leq m$), using $L^{(k)} = [x_k, y_k, z_k]$ to represent its location and t_{b0} as the initial clock bias, then the true distance r in the Equation (5) can be derived as $\|L^{(k)} - L_0\|$, and the measured pseudorange $\rho_0^{(k)}$ follows

$$\rho_0^{(k)} = \|L^{(k)} - L_0\| + ct_{b0} + \varepsilon_\rho \quad (7)$$

Next, we linearize the above equation. Assuming that the true position is $L = L_0 + \delta L$, the difference between the true position, which is the target of this algorithm, and the initial position can be derived as

$$\begin{aligned} \delta\rho^{(k)} &= \rho^{(k)} - \rho_0^{(k)} \\ &= \|\|L^{(k)} - (L_0 + \delta L)\| - \|L^{(k)} - L_0\| + c(t_b - t_{b0}) + \varepsilon_\rho \quad (8) \\ &\approx -\frac{L^{(k)} - L_0}{\|L^{(k)} - L_0\|} \delta L + c\delta t_b + \varepsilon_\rho = -I^{(k)} \delta L + c\delta t_b + \varepsilon_\rho \end{aligned}$$

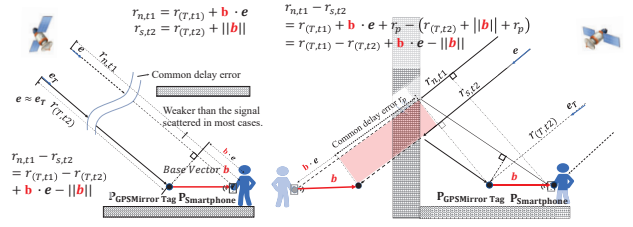
which present that $\delta\rho^{(k)}$ and δL are linearly related. Therefore, both pseudorange measurements from real satellites and virtual satellites can be linearized using Equation (8).

Different from conventional GPS algorithms which simply apply the WLS solver with these measurements, the position estimation equations are reconstructed with the extracted delay of scattered signals. Specifically, suppose we obtain two consecutive pseudorange measurements, $\rho^{(k,n)}$, from non-scattered GPS signals, and $\rho^{(k,s)}$, from GPSMirror, which can be regarded as the signal from virtual satellites. Let δt_{b1} be the clock bias directly from the satellites and $\delta t_{b2} = \delta t_{b1} + t_s$ be the estimated clock bias, where δt_{b2} is the true clock bias and t_s is the propagation delay through GPSMirror node. If we obtain k measurements $\mathbf{P}_n = [\rho^{(1,n)}, \dots, \rho^{(k,n)}]^T - \rho_0$ directly from the satellite and m measurements $\mathbf{P}_s = [\rho^{(1,s)}, \dots, \rho^{(m,s)}]^T - \rho_0$ from the GPSMirror node, We can organize the pseudorange of all measurements as

$$\delta\rho = \begin{bmatrix} \mathbf{P}_n \\ \mathbf{P}_s \end{bmatrix} = \begin{bmatrix} -\mathbf{I}_n^T & 1 & 0 \\ -\mathbf{I}_s^T & 0 & 1 \end{bmatrix} \begin{bmatrix} \delta L \\ c\delta t_{b1} \\ c\delta t_{b2} \end{bmatrix} + \varepsilon_\rho, \quad (9)$$

Then, we can estimate the δL through WLS:

$$\begin{bmatrix} \delta L \\ c\delta t_{b1} \\ c\delta t_{b2} \end{bmatrix} = ((G^T W G)^{-1} G^T W \delta\rho) \quad (10)$$



(a) Eliminate the common delay error in LoS. (b) Eliminate the common delay error in NLoS.

Figure 11: Typical use cases of a GPSMirror tag in shadowed regions.

where W is the weight of each equation from the measurement uncertainties. Then we obtain the true position $L = L_0 + \delta L$. Since t_s can be extracted by comparing pairs of scattered and non-scattered GPS signals from the same satellites. Therefore, in the best case, a single GPSMirror tag can help smartphone positioning with only two visible satellites after t_s has been extracted. If the number of satellites exceeds 2, we also can improve the accuracy with extra measurements.

4.3 Differential Positioning for Accuracy Improvement

The other problem in the shadowed regions is NLoS propagation. Intuitively, the lack of LoS leads to rapid degradation of positioning accuracy. Since the LoS from the satellites to GPSMirror tags and LoS from GPSMirror tags to smartphones are relatively easily guaranteed, an important question is: can we convert the legacy positioning method that requires LoS from the receiver to satellites into a positioning method that requires LoS to a GPSMirror tag?

Our basic idea is to cast the GPSMirror tags as reference stations, which create deterministic multipath to improve positioning accuracy and mitigate the errors caused by random ambient reflections. Unlike conventional reference station-based systems (e.g., DGPS [36]) that the stations can process and compute the propagation delays correctly and deliver them to smartphones, the low-power GPSMirror tags with limited resources cannot process GPS signals or tell the propagation delays. Thus, GPSMirror needs to extract distance measurements and finish the computation on smartphones. Since the satellites are far from the ground (about 20000 km), scattered and non-scattered GPS signals from the same satellite in a short interval can be considered as arriving in parallel with the common propagation errors, which are mainly caused by NLOS in shadowed regions. We cast the GPSMirror tags as reference stations to eliminate these errors.

Different from DGPS stations, GPSMirror tags cannot process GPS signals and extract errors of the referenced propagation path directly. We need to process signals from referenced propagation path and eliminate the propagation error

on smartphones. Following are detailed steps. As shown in Figure 11, we use a GPSMirror tag to scatter GPS signals to a smartphone and differential the distance measurements of scattered and non-scattered GPS signals to eliminate the common delay error. Specifically, suppose we obtain two nearby samples of carrier phase measurements, $\Phi_{n,t1}$ from non-scattered GPS signal at $t1$ and $\Phi_{s,t2}$ from scattered signals of the same satellite at $t2$. During this short interval, the angle of arrived GPS signal changes negligibly [40]. Therefore, we can assume that nearby samples of scattered and no-scattered GPS signals share the same common error, including the delay caused by reflection and atmospheric delay I and T .

Further, we can differentiate these measurements from scattered and non-scattered GPS signals to eliminate the common errors that compromise positioning accuracy. Specifically, We can acquire $\Phi_d = \Phi_{s,t2} - \Phi_{n,t1}$, in which $\Phi_{s,t2}$ is the distance measurements from scattered GPS signals and $\Phi_{n,t1}$ from non-scattered GPS signals of the same satellites. According to (6) can be expressed by

$$\Phi_d = r_{s,t2} - r_{n,t1} + c\Delta T + \Delta N + \varepsilon_\Phi \quad (11)$$

where ΔN is the difference of the phase offset and remains constant when the carrier phase is locked, both $r_{s,t2}$ and $r_{n,t1}$ are the distance between the same satellite to the smartphone at a different time. $\Delta T = (t_{R,t2} - t_{R,t1}) - (t_{S,t2} - t_{S,t1})$ is the difference of clock bias between the 2 measurements. As the clocks of satellites are stable, ΔT mainly depends on the stability of the local clock of smartphones.

Different from conventional DGPS stations, GPSMirror cannot estimate the Φ_d . Thus, we model an unknown vector \mathbf{b} to stand for a position vector from the tag to the smartphone and estimate it on the smartphone. As shown in Figure 11, we use $r_{T,t2}$ to denote the distance from the satellite to the GPSMirror tag from scattered GPS signals. Then we can presume $r_{s,t2} = r_{T,t2} + \|\mathbf{b}\|$ based on the geometric relationship in Figure 11. Further, we can acquire $r_{n,t1} = r_{T,t1} + \mathbf{b} \cdot \mathbf{e}$, where \mathbf{e} is the unit directional vector from the satellite to the smartphone and Φ_d can be expressed as

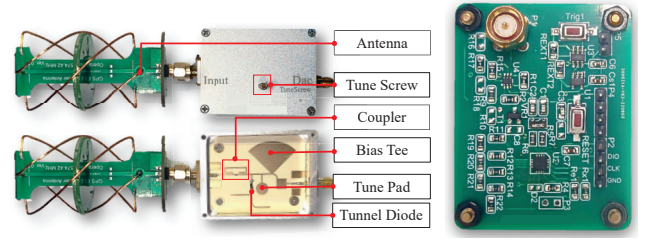
$$\Phi_d = \Delta r_T + \|\mathbf{b}\| - \mathbf{b} \cdot \mathbf{e} + c\Delta T + \lambda\Delta N + \varepsilon_\Phi \quad (12)$$

where $\Delta r_T = r_{T,t2} - r_{T,t1}$ is the distance from the satellites to the GPSMirror changes between $t1$ and $t2$. So far we obtained the relation between the measurements and the base vector \mathbf{b} . Then we re-organized the equation by placing the known quantities on the left side of the equation.

$$\begin{aligned} \Phi_d - \Delta r_T - \lambda\Delta N - \lambda\varphi_T &= \|\mathbf{b}\| - \mathbf{b} \cdot \mathbf{e} + c\Delta T + \varepsilon_\Phi \\ &= \sqrt{\mathbf{b}^T \mathbf{b}} - \mathbf{b} \cdot \mathbf{e} + c\Delta T + \varepsilon_\Phi \end{aligned} \quad (13)$$

In order to solve \mathbf{b} , we linearize this equation using Newton's iterative method. Given a \mathbf{b}_0 for initialization, the Equation (13) can be approximately expressed by

$$\begin{aligned} \Phi_d - \Delta r_T - \lambda\Delta N &\approx \sqrt{\mathbf{b}_0^T \mathbf{b}_0} - \mathbf{b}_0 \cdot \mathbf{e} + \frac{\partial(\sqrt{\mathbf{b}^T \mathbf{b}} - \mathbf{b} \cdot \mathbf{e})}{\partial \mathbf{b}} \delta \mathbf{b} \\ &+ c\Delta T + \varepsilon_\Phi \end{aligned} \quad (14)$$



(a) RF front-end of GPSMirror tags.

(b) Control circuit that provide bias voltage.

Figure 12: GPSMirror prototype.

We use $S_\Phi = \Phi_d - \Delta r_T - \lambda\Delta N - \sqrt{\mathbf{b}_0^T \mathbf{b}_0} + \mathbf{b}_0 \cdot \mathbf{e}$ to represent the known quantities. The Equation (14) can be re-organized as

$$S_\Phi = \frac{\partial(\sqrt{\mathbf{b}^T \mathbf{b}} - \mathbf{b} \cdot \mathbf{e})}{\partial \mathbf{b}} \delta \mathbf{b} + c\Delta T + \varepsilon_\Phi \quad (15)$$

Now according to Equation (15), the measured phase of GPS signals can be simply determined by the \mathbf{b} from the GPSMirror tag to the smartphone, which eliminates the requirement for LoS satellites. An intuitive explanation is that since the tag's position is known and the position of satellites can also be calculated based on the orbit information, the propagation path between satellites and the GPSMirror tag is derived indirectly.

Then we start to solve the base vector \mathbf{b} with multiple functions. We can obtain the base vector \mathbf{b} by estimating the $\delta \mathbf{b}$ since they are linearly related. There are 4 variable in Equation (15), $\mathbf{b} = [\mathbf{X}_{Smartphone} - \mathbf{X}_{Tag}, \mathbf{Y}_{Smartphone} - \mathbf{Y}_{Tag}, \mathbf{Z}_{Smartphone} - \mathbf{Z}_{Tag}]$ and ΔT . So 4 independent equations can help solve for \mathbf{b} . After we obtain $n \geq 4$ equations, we have

$$\mathbf{S}_\Phi = \begin{bmatrix} S_\Phi^{(1)} \\ \vdots \\ S_\Phi^{(n)} \end{bmatrix} = \begin{bmatrix} \frac{\partial(\sqrt{\mathbf{b}^T \mathbf{b}} - \mathbf{b} \cdot \mathbf{e})}{\partial \mathbf{b}} & 1 \\ \vdots & \vdots \\ \frac{\partial(\sqrt{\mathbf{b}^T \mathbf{b}} - \mathbf{b} \cdot \mathbf{e})}{\partial \mathbf{b}} & 1 \end{bmatrix} \begin{bmatrix} \delta \mathbf{b} \\ c\Delta T \end{bmatrix} + \varepsilon_\rho, \quad (16)$$

Then, we can estimate the $\delta \mathbf{b}$ through the WLS estimation equation as

$$\begin{bmatrix} \delta \mathbf{b} \\ c\Delta T \end{bmatrix} = ((G^T W G)^{-1} G^T W \mathbf{S}_\Phi) \quad (17)$$

We then update $\mathbf{b}_0 = \mathbf{b}_0 + \delta \mathbf{b}$ and iterate until the $\delta \mathbf{b}$ less than a preset threshold. Then we can obtain the estimated base vector \mathbf{b} . Further, since the location of GPSMirror tags and the floor plan is known after deployment, we filter out outlier \mathbf{b} with impossible directions to further improve accuracy. Finally, we obtain the position of the smartphone with $P_{Smartphone} = P_{GPSMirrorTag} + \mathbf{b}$ as shown in Figure 11.

5 SYSTEM IMPLEMENTATION

In this section, we describe the implementation of GPSMirror, including fabrication of GPSMirror tags, and GPS data logger on receivers, i.e., smartphones.

5.1 GPSMirror Tags.

To provide accurate, stable and configurable bias voltage for the tunnel diode with off-the-shelf components, we prototype each GPSMirror tag with the following components: a tunnel diode to provide negative resistance for GPS signal amplification, a DAC to provide accurate bias Voltage for the tunnel diode, a voltage reference chip that provides voltage reference against voltage-drift of the circuit, an MCU configures and controls other components, a voltage buffer to holds the bias when other components are shut down to save energy and a low dropout regulator (LDO) that provides energy for above components.

To facilitate manufacturing and commissioning, we divide the above components into two circuits. One is the front-end circuit that handles the RF signals with a tunnel diode and micro-strip lines, the other is the baseband control circuit that configures the bias voltage for the tunnel diode. As shown in Figure 12 (a), we fabricate the front-end circuit on a low-loss Rogers 4350B substrate with an immersion gold craft to reduce the impact of surface roughness and oxidation on impedance. Each circuit is fixed in a customized metal cavity to avoid ambient electromagnetic noise. Shown in Figure 12 (b) is the baseband control circuit fabricated on FR4. Besides, we also build the customized antenna with FR4 printed circuit board and copper wires.

Table 1: GPSMirror Cost Breakdown.

Components	Model	Price
Tunnel Diode	MBD1057	\$45.2
MCU	KL03Z16	\$2.99
Timer	TPL511DDCR	\$0.30
Voltage Buffer	LTC2063SC6	\$1.38
Voltage Reference	REF3012	\$0.45
DAC	MAX5531	\$4.34
LDO	TPS78218DDCT	\$0.50
Total	-	\$55.16

Cost. Table 1 is the latest detailed breakdown of cost based on quotes for 1000 units, where the unit cost is around \$55.16, but only \$9.96 if excluding the tunnel diode. Tunnel diodes contribute to 82% of the total cost due to the lack of market demand. If GPSMirror were successfully promoted and widely deployed, mass production would further lower the unit price of tunnel diodes.

Power Consumption. The tunnel diode consumes approximately $126 \mu\text{W}$ according to Figure 3 and the off-the-shelf LDO consumes approximately $1.6 \mu\text{W}$. To reduce overall energy consumption, the MCU and DAC operate duty-cycled to provide precise voltage output and the voltage buffer helps to hold the bias voltage for the tunnel diodes when the MCU and DAC are shut-down. The scattering control and configuration of DAC can be finished within 10 ms, thus the average power consumption of all these components is as low as $0.9 \mu\text{W}$. The voltage buffer consumes $6 \mu\text{W}$ and the total power consumption is approximately $134.5 \mu\text{W}$. $134.5 \mu\text{W}$ -power-consumption can enable the GPSMirror continuous work

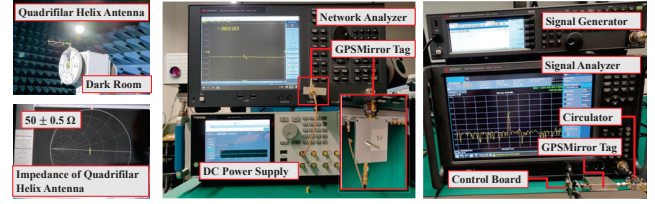


Figure 13: Hardware testbed.

for about 31 months with a coin-battery CR2477, which is also used in duty-cycled iBeacon [7] for a maximum of 24 months, while GPS relays/repeaters consume W-level power and require a plug-in supply. In addition, since distance measurements can be derived from any 1 ms-long GPS signal [27], the tunnel diode can also operate in duty-cycled mode to amplify GPS signals. GPSMirror tags can achieve battery-free with RF or PV energy harvesters like other backscatter systems.

5.2 Receiver.

We use various smartphones including XIAOMI 8, HUAWEI Mate20 Pro and SAMSUNG Galaxy S20 Ultra with the Gns-Logger 3.0 [17] app installed, which are used for data recording. We process the data and calculate the localization offline.

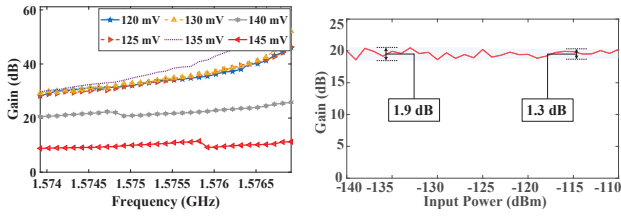
6 EVALUATION

In this section, we first evaluate the hardware performance of the GPSMirror tags with signal analyzers and smartphones. Then we conduct a series of experiments to test its coverage and localization performance under different conditions.

6.1 Experimental Setup.

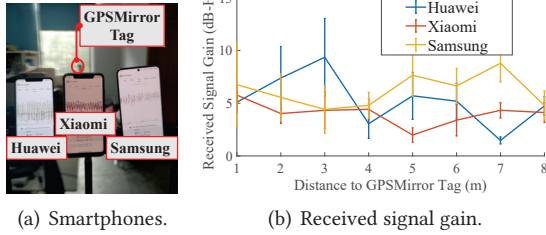
Hardware Testbed. The hardware testbed is used to profile the GPSMirror tag, including the gains in the L1 band, the impedance of antennas, and the front-end circuit. As shown in Figure 13 (b), we use the network analyzer E5061B in an electromagnetic darkroom to measure the impedance and radiation pattern of the antenna and to tune the antenna to 50 ohms in the L1 band. The network analyzer N5225B is used to measure the reflection coefficient of the tag with a weak excitation power. The AWG 5000 arbitrary waveform generator provides accurate bias voltages to the GPSMirror tags. We use the Keysight MXG analog signal generator N5182B and the Keysight UXA signal analyzer N9020A to measure the gain of the GPSMirror tags. N5182B can generate RF signals as low as -140 dBm, and N9020A has a typical sensitivity of -150 dBm.

Ground Truth. We use a Xiaomi LS-P laser range finder with a range error of 3 mm to obtain the ground truth for distance measurements. We use a Unistrong P40 board in real-time kinematic positioning (RTK) mode to obtain the ground truth for coordinates measurements. The position error of the



(a) Gain vs Bias Voltage.

(b) Gain vs Input Power.

Figure 14: Hardware performance of a GPSMirror tag.

(a) Smartphones.

(b) Received signal gain.

Figure 15: Reception on various smartphones.

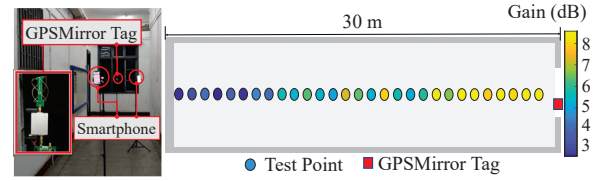
Unistrong P40 in RTK mode is 8 mm when synchronized with differential stations. However, the Unistrong P40 board often fails to sync when it gets close to buildings or flyovers. We thus measure the coordinates of test points at least 30 meters away from buildings and derive all the required coordinates based on the distances measured by the laser range finder.

Deployment of GPSMirror tags. The GPSMirror tags can be deployed outside the building, in openings of a building or in unenclosed parts of flyovers to provide GPS service for pedestrians. The locations of the GPSMirror tags are registered in the map or floor plan and stored in the GPSMirror's database on smartphones.

6.2 GPS Signal Re-radiation

Performance Profiling with Hardware Testbed. To measure the gain of the GPSMirror tag, we use the signal generator to generate a -140 dBm RF signal that passes through the GPSMirror tag to the spectrum analyzer. The gain is obtained by comparing the signal strength of the signal generator's output and the measured signal strength of the signal analyzer. The results are presented in Figure 14(a), where we can see the GPSMirror tag achieves about 22 dB gain with negligible distortion when the bias voltage is set at 140mV and higher gains are reachable with the bias voltage changes. We also evaluated the gain with different input signal power and the results are presented in Figure 14(b), where we can see the GPSMirror tag achieves flat gain with distortions less than 1.3 dB when the input power higher than -125 dBm and 1.9 dB when input power higher than -140 dBm. Thus, we can conservatively conclude that the GPSMirror tag has sufficient sensitivity (≤ -125 dBm) to scatter GPS signals.

Received Signal Quality on Smartphones. We test the signal quality on three different smartphones, including Samsung Galaxy S20, Huawei Mate20 Pro and Xiaomi 8, to verify

**Figure 16: Coverage test in a corridor.**

the compatibility. As shown in the Figure 15, we deploy a GPSMirror tag near a window and use three smartphones to record data simultaneously, with a distance to the tag ranging from 1 m to 8 m. Results show that smartphones from different manufacturers can achieve effective reception of GPSMirror scattered signals without significant differences.

6.3 Coverage of GPSMirror Tags

We define the coverage as the region where a GPSMirror tag's "ON-OFF" switching can be detected and smartphones can position with the tag. GPSMirror enhances the GPS coverage in two main aspects. On the one hand, GPSMirror tags alter the propagation paths to increase the number of visible satellites. On the other hand, the GPS signals originally reachable to GPS receivers are strengthened by the GPSMirror tags. To evaluate the coverage performance from both aspects, we deploy GPSMirror tags in various scenarios including a 30m-long corridor, a $50 \times 12 m^2$ sidewalk in an urban canyon, a $17.5 \times 12 m^2$ classroom and a $20 \times 14 m^2$ lecture hall. We set test points in each scenario and use smartphones to record raw C/N_0 measurements of scattered and non-scattered GPS signals for 5 minutes at each test point. We use the C/N_0 of scattered GPS signals to minus that of non-scattered signals to stand for the enhancement performance. Then we plot the mean value of 5 minutes in each test point as shown from Figure 16 to Figure 19.

In all scenarios, GPSMirror tags strengthen the GPS signal by at least 3 dB including the farthest location. Specifically, at the farthest test point in Figure 17, which is 27.7 m away from the tag, there is >4 dB gain from the tag in both wall-mounted and tripod-mounted conditions. Since the nearest test point is about 2 m to the tag with gains of 9 dB, the drop-off of the gain is about 5 dB in this condition. Moreover, the farthest test point in Figure 19 is about 15.6 m to the tag with >3 dB in the three conditions. Therefore we can conclude that the gain's drop-off is slow. Besides, Figure 16 shows that the GPSMirror tag can enable sufficient coverage with a radius of up to 30 m. Thus, the coverage of GPSMirror tags reaches the limit of the US regulation [47], i.e., 30 m.

Impact of Mounting Methods. To evaluate the impact of different mounting methods, we conduct experiments to evaluate the performance of wall-mounted, window-mounted and tripod-mounted tags in both indoor and outdoor scenarios. Specifically, the Figure 17 shows the coverage performance of a GPSMirror tag with different mounting methods

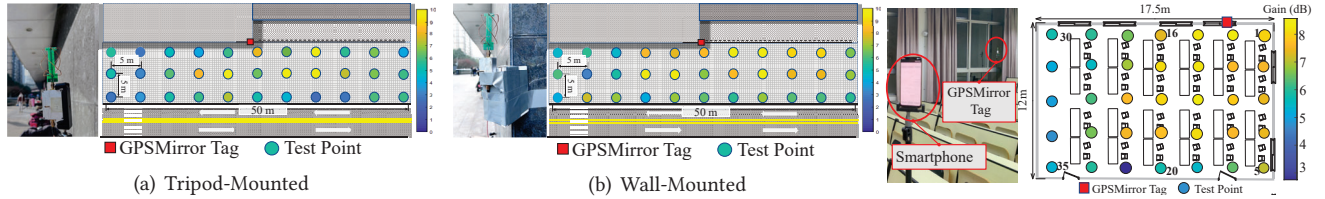


Figure 17: Coverage performance of a GPSMirror Tag in urban canyon. Figure 18: Coverage test in a room.

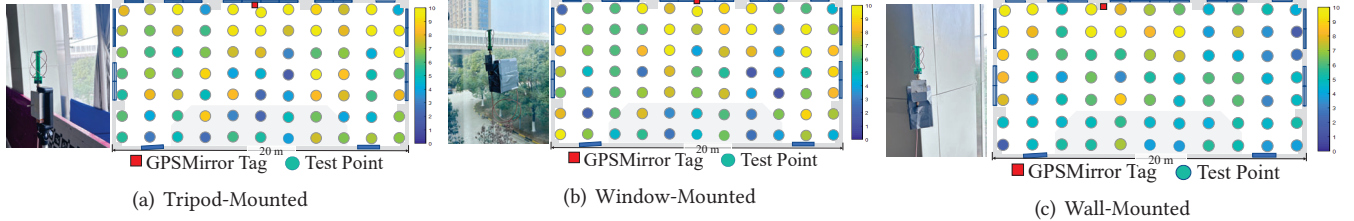


Figure 19: Coverage performance of a GPSMirror tag with different mounting methods in a flat room.

in an urban canyon. We set 33 test points and each point spaced 5 m apart. Figure 19 shows the coverage of GPSMirror tags in a lecture hall with different mounting methods. We set 77 test points and each one is spaced 2 m apart. Results show that different mounting methods have a negligible impact on the coverage.

Impact of Deployment Location. We notice that the deployment location of the GPSMirror tag influences the gain's distribution in these test points. We compare Figure 19(a),19(b) and Figure 19(c) can draw a conclusion that it is better to deploy the GPSMirror tag close to the center of the open area for more uniform signal enhancement.

6.4 Positioning Accuracy

To fully exploit the performance of positioning accuracy, we conduct the following experiment to evaluate the performance of both static and dynamic positioning. Further, we conduct a controlled experiment to explore the potential of using multiple GPSMirror tags for high positioning accuracy.

Static positioning. We evaluate the static positioning accuracy of the GPSMirror system in the following two scenarios: indoors, as shown in the Figure 18 and 19, and in an urban canyon, as shown in the Figure 17. To assess performance, we plot the cumulative distribution function (CDF) using the average position error of each point. The median positioning error is about 3.7 m in the indoor scenario and 4.6 m in the urban canyon as plotted in Figure 20. The localization accuracy in the indoor scenario is a little better than that in urban canyons. We speculate that this effect may be caused by the following reason. The propagation path through a GPSMirror tag in an indoor scenario is more clear since windows are the only opening to the sky. On the contrary, GPS signals in an urban canyon are more complex since smartphones may receive more signals from propagation paths other than through the GPSMirror tags. Overall,

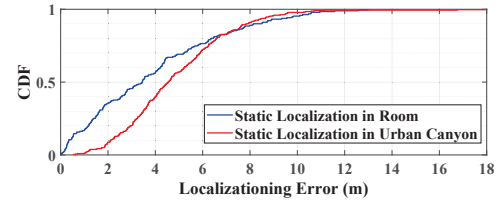


Figure 20: Positioning accuracy.

the accuracy in both scenarios improves a lot with a GPSMirror tag eliminating the common delay errors.

Dynamic positioning. To evaluate the performance of dynamic positioning, we perform a controlled experiment with a GPSMirror tag mounted on the window and set 3 types of trajectories for the receiver as shown in the Figure 21. A volunteer walks along the trajectories with an average speed of about 25 cm/s per second and holds a smartphone recording GPS measurements. We compute the location based on every four samples and compare it with the ground truth, which is distributed every 1 m on the trajectories. The results show that we can achieve a median localization error of about 4.5 m with GPS signals only, which is sufficient in urban canyons and some indoor regions. However, the accuracy gets a little worse than in static positioning conditions. We speculate this may be primarily limited by the low sampling rate of the smartphone, which is default set as 1 Hz for energy saving. We need multiple samples to eliminate the common error correctly, the correlation between these samples reduces more in dynamic localization conditions. Thus, the accuracy gets a little worse. This limitation can be mitigated by increasing the sampling rate. Some GNSS sensors for smartphones support higher sampling rates, e.g., 40Hz [48]. We can achieve the rate with firmware modifications [43].

Positioning with multiple Tags. To explore the potential of using multiple GPSMirror tags for further localization accuracy improvements, we conduct a controlled experiment

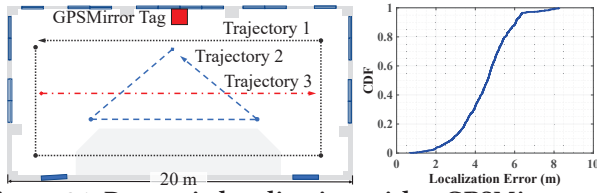


Figure 21: Dynamic localization with a GPSMirror tag.

with 2 tripod-mounted tags providing GPS-enhancing service simultaneously. The 2 tags are synchronized with a cable and operate with a time-division schedule. We set 3 test points and used a handheld smartphone to record 180 samples at each test point. We estimate the position of the smartphone with Tag1 and Tag2, then use both base vectors from the two tags to estimate the position of the smartphone. As shown in Figure 22, the average positioning accuracy of using two tags in the three test points are about 2.6 m, 2.4 m, and 3.6 m with error bars on 95 % confidence interval. The localization results with two tags perform better than that using one tag significantly.

6.5 Case Studies

We deploy the GPSMirror tags and evaluate the positioning accuracy of our system in four real-world scenarios, i.e., large flat room (Factory, Figure 23), flyover (Figure 24), Exterior of tall buildings (Urban canyon, Figure 25)), and center patio (Urban canyon, Figure 26). We use an open-source GPS position estimation project provided by Google as baseline [17].

Figure 23 shows the results in a large flat room on the ground, a common architectural structure as in many factories. We deploy a single GPSMirror tag in the room and evaluate the localization performance in 3 positions. Google’s baseline algorithm fails to position in test point 2 and 3 due to insufficient visible satellites. In contrast, GPSMirror achieves the positioning accuracy of under 10 m for all test points.

Figure 24 shows the results under a flyover, which is challenging for a single GPSMirror tag to provide GPS service. Because the middle is the vehicle way, the GPSMirror tag can only be deployed at one side, which is not the area that provides the best coverage. We evaluate the positioning performance in 2 test points. As expected, the positioning accuracy decreases on the other side of the road.

The exterior of tall buildings is a common view in urban areas. We deploy a single GPSMirror tag 12 m away from the building and try to provide high-accuracy GPS service near the building. In position 1 and position 3, GPSMirror achieves average performance while Google’s baseline algorithm degrades rapidly. However, the positioning accuracy of Google’s baseline in position 2 (LoS region) achieves better performance. This is as expected because the position is far from the GPSMirror tag while conventional GPS positioning algorithms can achieve good performance in LoS regions, which are not our target cases.

The center patio is a common architectural structure in an urban area, which is surrounded by tall buildings with only the middle part having a view of the sky. We deploy GPSMirror tags here to further evaluate the generalizability of our tags in downtown mega-cities. As shown in the Figure 26, GPSMirror significantly improved the position accuracy for all test points.

7 RELATED WORK

GPS relays. Commonly used GPS relays [13–15] mainly consist of two parts. The first part includes an antenna and an LNA deployed outdoors, to receive the signals from GPS satellites. The second part is deployed inside the building and consists of a GPS transmit antenna and a power amplifier. These two parts are connected by an RF cable and powered by a plug-in source. Such GPS relays are power hungry, typically consuming W -level power for coverage of less than 30 m [47]. They are not easy to deploy due to the need for a stable power supply and the complexity of routing RF cables. In contrast, GPSMirror re-radiates GPS signals by integrating an antenna and a reflection amplifier into a single module. It only consumes μW -level power and can be easily supplied by a coin battery or an energy harvesting module.

GPS and wireless positioning. Recent efforts [29, 32, 38] have attempted to improve the performance of GPS positioning. CO-GPS [29] designs a cloud-offloaded GPS solution to save energy for portable sensing devices. GNOME [32] proposes a novel vision-assisted algorithm leveraging Google Street View for accurate GPS positioning in urban canyons. COIN-GPS [38] develops a robust GPS receiver with a purpose-built directional antenna to achieve indoor GPS positioning. GPSMirror is inspired by this literature while aiming to provide practical indoor GPS positioning services for off-the-shelf smartphones. DGPS [36, 53] use one or more reference stations to eliminate the propagation errors for accurate positioning. GPSMirror shares similar principles to reduce positioning errors, but differs from DGPS in that the positioning algorithm runs entirely on unmodified smartphones, merely using the GPS service APIs.

Wireless indoor positioning systems, such as Bluetooth low energy (BLE) [6, 8, 23], ultra-wide-band (UWB) [10, 11, 41, 55], and WiFi [22, 24], have demonstrated high precision for indoor localization. However, such specialized infrastructures entail laborious mapping and calibration at the deployment phase and also require a power supply for continuous positioning. They are not compatible with the GPS service on smartphones and have not seen wide deployment.

Tunnel diode-based backscatter. Recent research demonstrated that tunnel diodes enable orders of magnitude improvement in backscatter communication range with μW -level power consumption [4, 5, 19, 50–52]. GPSMirror also uses a tunnel diode to amplify incident signals, but differs

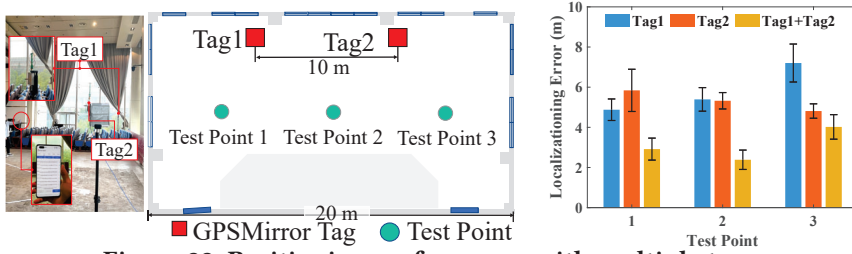


Figure 22: Positioning performance with multiple tags.

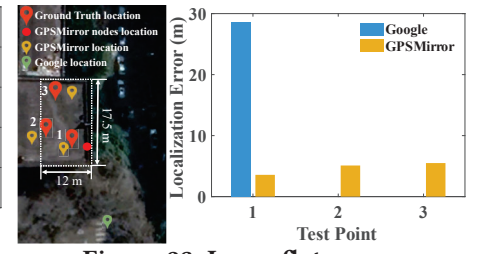


Figure 23: Large flat room.

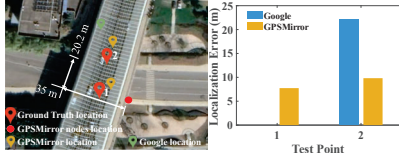


Figure 24: Under flyover.

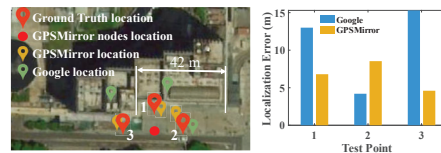


Figure 25: Exterior of buildings.

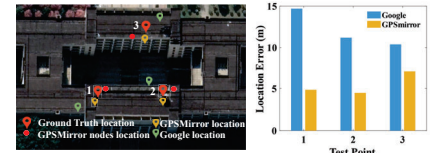


Figure 26: Center patio.

from the prior work through new noise suppression and precision impedance control mechanisms. Specifically, GPSMirror needs to be highly sensitive in acquiring weak GPS signals and to ensure that the scattered signals still preserve the modulated waveforms of incident signals. The backscatter design in GPSMirror is the first to meet these requirements. Moreover, GPSMirror strictly works as a reflective amplifier rather than a tunnel diode oscillator [4, 5, 19, 50, 51]. GPSMirror does not need to generate a carrier by itself because it only captures and amplifies the GPS signals. Jodu [52] also employs a tunnel diode to achieve a reflective amplifier for communication. However, it cannot be applied to GPSMirror because it suppresses the harmonics of carriers to reduce interference. The harmonics suppression would lead to distortion of GPS signals since GPS signals are spectrum-spread.

8 DISCUSSION

Positioning error. GPSMirror demonstrates significant improvement in localization accuracy compared to other GPS solutions, however, there is still room for further improvement to reduce positioning errors. The source of the positioning error of GPSMirror may include (i) the average user range error (URE) set by government limitations, which is approximately 0.6m [18], (ii) wrong measurements due to low SNR, (iii) insufficient spatial diversity with the use of a single tag. The limitations (i) and (ii) are fundamental to GPS signals, while (iii) can be addressed through the deployment of multiple tags. Additionally, the accuracy can be further improved through the use of continuous-time Kalman filters and sensor-fusion techniques.

Deployment cost. The GPSMirror has several advantages over traditional GPS relays/repeaters in terms of cost efficiency for deployment. First, GPSMirror does not need a plug-in power supply, which can significantly reduce system deployment and maintenance costs. Second, GPSMirror costs \$55.16 and 82% of the tag's cost comes from tunnel diodes, which will further "reduce cost if developed at scale" [50],

while a GPS relay/repeater system costs \$1209 [14] or \$1224 [13] with similar coverage under regulations. Besides, GPSMirror also has a lower deployment cost than BLE beacons in GPS-shadowed regions. Typically, only one GPSMirror tag is needed to provide positioning services for smartphones, whereas at least three BLE beacons are required for the same purpose. The cost of a GPSMirror tag is cheaper than BLE beacons (such as an iBeacon, which costs \$69 [7] for 3). Therefore, GPSMirror is more cost-efficient for deployment.

9 CONCLUSION

We designed and validated GPSMirror, an ultra-low power system to expand accurate GPS positioning to shadowed and indoor regions for smartphones. The key enabling hardware in GPSMirror is the first high sensitive backscatter that can re-radiate extremely weak GPS signals and provide enough coverage that approaches the regulation limit. Beyond GPS positioning, we also envision the GPSMirror design can be adapted to accommodate a wider range of use cases, such as satellite communications through backscatter.

10 ACKNOWLEDGMENTS

We thank our shepherd and reviewers for their helpful feedback, which greatly improved the quality of the paper. This work was supported in part by the National Key R&D Program of China under Grant 2020YFB1806600, the National Science Foundation of China with Grant 62071194, the Key R&D Program of Hubei Province of China under Grant No. 2021EHB002, the Knowledge Innovation Program of Wuhan-Shuguang, the European Union's Horizon 2020 research and innovation programme under the Marie Skłodowska-Curie grant agreement No 101022280 and No 824019.

REFERENCES

- [1] Aeroflex. 2012. MBD1057 Datasheet. [http://pdf.datasheet.live/datasheets-1/aeroflex_\[metelics\]/MBD1057-C18.pdf](http://pdf.datasheet.live/datasheets-1/aeroflex_[metelics]/MBD1057-C18.pdf).
- [2] Fahim Ahmed, Mark Phillips, Stephen Phillips, and Kyoung-Yun Kim. 2020. Comparative study of seamless asset location and tracking

- technologies. *Procedia Manufacturing* 51 (2020), 1138–1145.
- [3] SL Altman. 1986. Rotations, quaternions, and double groups. Clarendon.
- [4] Francesco Amato and Gregory D Durgin. 2018. Tunnel diodes for backscattering communications. In *2018 2nd URSI Atlantic Radio Science Meeting (AT-RASC)*. IEEE, 1–3.
- [5] Francesco Amato and Simon Hemour. 2019. The harmonic tunneling tag: A dual-band approach to backscattering communications. In *2019 IEEE International Conference on RFID Technology and Applications (RFID-TA)*. IEEE, 244–247.
- [6] Roshan Ayyalasomayajula, Deepak Vasisht, and Dinesh Bharadia. 2018. BLoc: CSI-Based Accurate Localization for BLE Tags. In *Proceedings of the 14th International Conference on Emerging Networking Experiments and Technologies (Heraklion, Greece) (CoNEXT '18)*. Association for Computing Machinery, New York, NY, USA, 126–138. <https://doi.org/10.1145/3281411.3281428>
- [7] Beaconstac. [n. d.]. iBeacon Technology. [EB/OL]. <https://www.beaconstac.com/apple-ibeacon-technology> Accessed Jan, 2023.
- [8] BeaconTrax. 2022. Trax20220. <https://www.beacontrax.com/product/trax20220-bluetooth-lte-m-ble-gateway/>.
- [9] Kongyang Chen and Guang Tan. 2018. BikeGPS: Accurate Localization of Shared Bikes in Street Canyons via Low-Level GPS Cooperation. In *Proceedings of the 16th Annual International Conference on Mobile Systems, Applications, and Services (MobiSys '18)*. Association for Computing Machinery, New York, NY, USA, 150–162. <https://doi.org/10.1145/3210240.3210316>
- [10] Ashutosh Dhekne, Ayon Chakraborty, Karthikeyan Sundaresan, and Sampath Rangarajan. 2019. TrackIO: Tracking First Responders Inside-Out. In *16th USENIX Symposium on Networked Systems Design and Implementation*. USENIX Association, Boston, MA, 751–764. <https://www.usenix.org/conference/nsdi19/presentation/dhekne>
- [11] EHIGH. 2016. EHIGH EH100602D04 Datasheet. <https://www.ehighwb.com/product-item-11.html>.
- [12] Farhad Farzami, Seiran Khaledian, Bisma Smida, and Danilo Erricolo. 2017. Ultra-low power reflection amplifier using tunnel diode for RFID applications. In *2017 IEEE International Symposium on Antennas and Propagation & USNC/URSI National Radio Science Meeting*. IEEE, 2511–2512.
- [13] gemsnav. 2016. RGA30-DV GPS relay. http://en.gemsnav.com/product_detail_10.html.
- [14] gemsnav. 2019. GRK-1 GPS relay. http://www.gemsnav.com/product_detail_60.html.
- [15] gemsnav. 2019. Q-GL1 GPS relay. http://www.gemsnav.com/product_detail_16.html.
- [16] geomax positioning. 2018. GNSS Receiver Zenith35 Pro Series. <https://geoprema.com/products/survey-equipment/survey-gps-gnss/geomax-zenith-35-pro-gps-gnss/>.
- [17] Google. 2016. GPS Measurement Tools. <https://github.com/google/gps-measurement-tools>.
- [18] Official U.S. government information about the GPS and related topics. 2020. GPS Accuracy. <https://www.gps.gov/systems/gps/performance/accuracy/>.
- [19] Karan Gumber, Francesco Amato, Corinne Dejous, and Simon Hemour. 2020. Nonlinear negative resistance-based harmonic backscatter. In *2020 IEEE/MTT-S International Microwave Symposium (IMS)*. IEEE, 603–606.
- [20] HSE Booklet HSG47. 2000. Avoiding Danger from Underground Services. <https://www.spenergynetworks.co.uk/userfiles/file/hsg47.pdf>.
- [21] Todd E Humphreys, Matthew Murrin, Frank Van Diggelen, Sergei Podshivalov, and Kenneth M Pesyna. 2016. On the feasibility of cm-accurate positioning via a smartphone's antenna and GNSS chip. In *2016 IEEE/ION position, location and navigation symposium (PLANS)*. IEEE, 232–242.
- [22] Mohamed Ibrahim, Hansi Liu, Minitha Jawahar, Viet Nguyen, Marco Gruteser, Richard Howard, Bo Yu, and Fan Bai. 2018. Verification: Accuracy evaluation of WiFi fine time measurements on an open platform. In *Proceedings of the 24th Annual International Conference on Mobile Computing and Networking*. 417–427.
- [23] Texas Instrument. 2016. CC2640R2F Datasheet. <https://www.ti.com/product/CC2640R2F>.
- [24] Texas Instrument. 2020. CC3230S Datasheet. <https://www.ti.com/product/CC3230S>.
- [25] Junsu Jang and Fadel Adib. 2019. Underwater backscatter networking. In *Proceedings of the ACM Special Interest Group on Data Communication*. 187–199.
- [26] AK Jonscher. 1961. The physics of the tunnel diode. *British Journal of Applied Physics* 12, 12 (1961), 654.
- [27] M Kayton. 2002. Global positioning system: signals, measurements, and performance [Book Review]. *IEEE Aerospace and Electronic Systems Magazine* 17, 10 (2002), 36–37.
- [28] J-L Li, S-W Qu, and Quan Xue. 2009. Compact microstrip lowpass filter with sharp roll-off and wide stop-band. *Electronics Letters* 45, 2 (2009), 110–111.
- [29] Jie Liu, Bodhi Priyantha, Ted Hart, Yuzhe Jin, Woosuk Lee, Vijay Raghunathan, Heitor S Ramos, and Qiang Wang. 2015. CO-GPS: Energy efficient GPS sensing with cloud offloading. *IEEE Transactions on Mobile Computing* 15, 6 (2015), 1348–1361.
- [30] Vincent Liu, Aaron Parks, Vamsi Talla, Shyamnath Gollakota, David Wetherall, and Joshua R Smith. 2013. Ambient backscatter: Wireless communication out of thin air. *ACM SIGCOMM Computer Communication Review* 43, 4 (2013), 39–50.
- [31] Vincent Liu, Vamsi Talla, and Shyamnath Gollakota. 2014. Enabling instantaneous feedback with full-duplex backscatter. In *Proceedings of the 20th annual international conference on Mobile computing and networking*. 67–78.
- [32] Xiaochen Liu, Suman Nath, and Ramesh Govindan. 2018. Gnome: A practical approach to nlos mitigation for gps positioning in smart-phones. In *Proceedings of the 16th Annual International Conference on Mobile Systems, Applications, and Services*. 163–177.
- [33] Marty McCann. 2009. DSP Presets and Power Amplifier Voltage Gain. <https://peavey.com/PDFs/Voltage-Gain-1.pdf>.
- [34] Oleg Mezentsev, Gerard Lachapelle, and Jussi Collin. 2005. Pedestrian dead reckoning—A solution to navigation in GPS signal degraded areas? *Geomatica* 59, 2 (2005), 175–182.
- [35] O Mezentsev, Y Lu, G Lachapelle, and R Klukas. 2002. Vehicular navigation in urban canyons using a high sensitivity GPS receiver augmented with a low cost rate gyro. In *Proceedings of the 15th International Technical Meeting of the Satellite Division of The Institute of Navigation (ION GPS 2002)*. 363–369.
- [36] GJ Morgan-Owen and GT Johnston. 1995. Differential GPS positioning. *Electronics & Communication Engineering Journal* 7, 1 (1995), 11–21.
- [37] G. T. Munsterman. 1965. Tunnel-Diode Microwave Amplifiers. <https://www.jhuapl.edu/Content/techdigest/pdf/APL-V04-N05/APL-04-05-Munsterman.pdf>.
- [38] Shahriar Nirjon, Jie Liu, Gerald DeJean, Bodhi Priyantha, Yuzhe Jin, and Ted Hart. 2014. COIN-GPS: indoor localization from direct GPS receiving. In *Proceedings of the 12th annual international conference on Mobile systems, applications, and services*. 301–314.
- [39] U.S. Department of Transportation. 2020. New York City Connected Vehicle Pilot Uses an Innovative Approach to Verify Location Accuracy in the City's Urban Canyons. https://www.its.dot.gov/pilots/nyc_cvp_canyons.htm.
- [40] Bradford W Parkinson and Per K Enge. 1996. Differential gps. *Global Positioning System: Theory and applications*. 2 (1996), 3–50.

- [41] Qorvo. 2017. DW1000 Datasheet. <https://www.qorvo.com/products/p/DW1000>.
- [42] ROGER. 2016. ROGER GPS Datasheet. <https://www.gps-repeating.com/products/gnss-repeaters/gnss-l1g1ga-gnss-repeater.html>.
- [43] Steven Shade and Premal H Madhani. 2018. Android GNSS Measurements-Inside the BCM47755. In *Proceedings of the 31st International Technical Meeting of the Satellite Division of The Institute of Navigation (ION GNSS+ 2018)*. 554–579.
- [44] Wang-Ik Son, Won-Gyu Lim, Moon-Que Lee, Sang-Bo Min, and Jong-Won Yu. 2008. Printed Square Quadrifilar Helix Antenna (QHA) for GPS Receiver. In *2008 38th European Microwave Conference*. 1292–1295. <https://doi.org/10.1109/EUMC.2008.4751699>
- [45] Vamsi Talla, Mehrdad Hesar, Bryce Kellogg, Ali Najafi, Joshua R Smith, and Shyamnath Gollakota. 2017. Lora backscatter: Enabling the vision of ubiquitous connectivity. *Proceedings of the ACM on Interactive, Mobile, Wearable and Ubiquitous Technologies* 1, 3 (2017), 1–24.
- [46] National Telecommunications and Information Administration. 2010. *Electromagnetic compatibility and Radio spectrum Matters (ERM); Short Range Devices; Global Navigation Satellite Systems (GNSS) Repeaters*.
- [47] National Telecommunications and Information Administration. 2013. *8.3.28 Use of Fixed Devices That Re-Radiate Signals Received From the Global Positioning System*. NTIA.
- [48] U-Blox. 2021. u-blox D9 correction data receiver. https://content.u-blox.com/sites/default/files/u-blox-D9-PMP-1.04_InterfaceDescription_UBX-21040023.pdf.
- [49] Frank van Diggelen. 2021. Improving urban GPS accuracy for your app. <https://android-developers.googleblog.com/2020/12/improving-urban-gps-accuracy-for-your.html>.
- [50] Ambuj Varshney and Lorenzo Corneo. 2020. Tunnel emitter: tunnel diode based low-power carrier emitters for backscatter tags. In *Proceedings of the 26th Annual International Conference on Mobile Computing and Networking*. 1–14.
- [51] Ambuj Varshney, Andreas Soleiman, and Thiemo Voigt. 2019. Tunnelscatter: Low power communication for sensor tags using tunnel diodes. In *The 25th Annual International Conference on Mobile Computing and Networking*. 1–17.
- [52] Ambuj Varshney, Wenqing Yan, and Prabal Dutta. 2022. Judo: addressing the energy asymmetry of wireless embedded systems through tunnel diode based wireless transmitters. In *Proceedings of the 20th Annual International Conference on Mobile Systems, Applications and Services*. 273–286.
- [53] Duojie Weng, Xingli Gan, Wu Chen, Shengyue Ji, and Yangwei Lu. 2020. A new DGNS positioning infrastructure for android smartphones. *Sensors* 20, 2 (2020), 487.
- [54] Ao Yariv and Jo So Cook. 1961. A noise investigation of tunnel-diode microwave amplifiers. *Proceedings of the IRE* 49, 4 (1961), 739–743.
- [55] Minghui Zhao, Tyler Chang, Aditya Arun, Roshan Ayyalasomayajula, Chi Zhang, and Dinesh Bharadia. 2021. ULoc: Low-Power, Scalable and Cm-Accurate UWB-Tag Localization and Tracking for Indoor Applications. *Proc. ACM Interact. Mob. Wearable Ubiquitous Technol.* 5, 3, Article 140 (sep 2021), 31 pages. <https://doi.org/10.1145/3478124>
- [56] Renjie Zhao, Purui Wang, Yunfei Ma, Pengyu Zhang, Hongqiang Harry Liu, Xianshang Lin, Xinyu Zhang, Chenren Xu, and Ming Zhang. 2020. Nfc+ breaking nfc networking limits through resonance engineering. In *Proceedings of the Annual conference of the ACM Special Interest Group on Data Communication on the applications, technologies, architectures, and protocols for computer communication*. 694–707.
- [57] Renjie Zhao, Fengyuan Zhu, Yuda Feng, Siyuan Peng, Xiaohua Tian, Hui Yu, and Xinbing Wang. 2019. OFDMA-enabled Wi-Fi backscatter. In *The 25th Annual International Conference on Mobile Computing and Networking*. 1–15.